J. Fluid Mech. (1979), *vol.* 91, *part* 4, *pp.* 633–659
Printed in Great Britain

Effects of small streamline curvature on turbulent duct flow

By I. A. HUNT† AND P. N. JOUBERT

Department of Mechanical Engineering, University of Melbourne, Parkville, Australia

(Received 15 October 1976 and in revised form 1 May 1978)

Mean velocity profiles, turbulence intensity distributions and streamwise energy spectra are presented for turbulent air flow in a smooth-walled, high aspect ratio rectangular duct with small streamwise curvature, and are compared with measurements taken in a similar straight duct.

The results for the present curved flow are found to differ significantly from those for the more highly curved flows reported previously, and suggest the need to distinguish between 'shear-dominated' flows with small curvature and 'inertia-dominated' flows with high curvature. Velocity defect and angular-momentum defect hypotheses fail to correlate the central-region mean flow data, but the wall-region data are consistent with the conventional straight-wall similarity hypothesis. A secondary flow of Taylor–Goertler vortex pattern is found to occur in the central flow region.

An examination of the flow equations yields a model for the mechanisms by which streamline curvature affects turbulent flow, in which a major effect is a direct change in the turbulent shear stress through a conservative reorientation of the turbulence intensity components. Data for the streamwise and transverse turbulence intensities show behaviour consistent with that expected from the equations, and the distribution of total turbulence energy in the central flow region is found to be nearly invariant with Reynolds number and wall curvature, in agreement with the model.

Energy spectra for the streamwise component are examined in terms of a Townsend-type two-component turbulence model. They indicate that a universal, 'active' component exists in all flow regions, with an 'inactive' component which affects only the low wavenumber spectra intensities. This is taken to imply that the effects of streamline curvature are determined by the central-region flow structure alone.

1. Introduction

The investigation reported here is an attempt to isolate and study the effects of small streamline curvature on a simple shear flow, that of air in a smooth-walled rectangular duct of sufficiently high aspect ratio that the mid-plane flow is essentially two-dimensional. The flow in a straight duct was examined first to provide a datum which the curvature effects could be assessed. The flow in a curved duct was then examined; the majority of the available data is restricted to mean flow studies of strongly curved flows, and neither these data nor the more sparse turbulence data indicate any clear means of quantifying the effects of curvature. The radius of curvature chosen for the present study was large compared with that of other investigations,

† Present address: Aeronautical Research Laboratories, Fishermen's Bend, Melbourne, Victoria, Australia.

0022-1120/79/4184-6070 $02.00

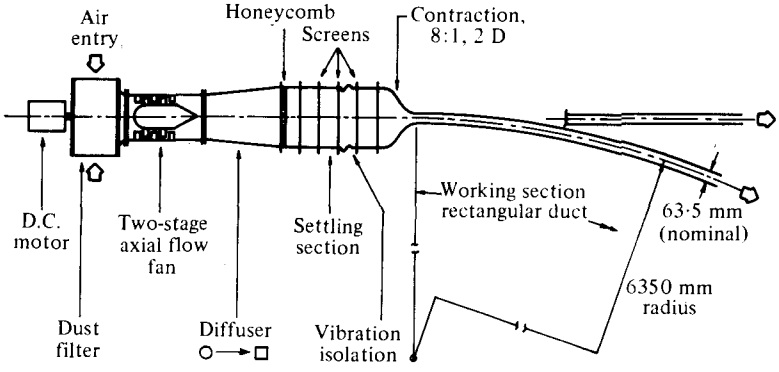

FIGURE 1. General arrangement of tunnel. Plan view, not to scale.

in an attempt to obtain a 'perturbed straight flow' rather than a flow dominated by the effects of streamline curvature. The curved duct was as far as practically possible identical with the straight duct in all respects except its curvature, and the flow in it was examined using identical instruments and techniques.

2. Apparatus and methods

2.1. *Duct details*

The open-return blower tunnel is shown in schematic form in figure 1. The ducts were formed by a single pair of stiffened acrylic-sheet side walls bolted to straight and curved pairs of extruded aluminium channel end walls. The total length of the duct was $75D$ (where D is the nominal duct width, 63·5 mm), the aspect ratio was 13·2 and the maximum Reynolds number obtainable was 190 000 (based on D and the maximum velocity U_m). The curved duct had a constant mean radius of curvature $\bar{r} = 100D$, and was mounted tangential to the tunnel centre-line at the contraction exit. The entry boundary layers were tripped by a row of pin-type stimulators on each wall at $2D$ from the contraction exit plane. Static pressure tappings and measurement stations were provided along the centre-line of each wall at multiples of D, measured from the contraction exit plane as origin, and complete access to the flow cross-section was obtained by inserting probes upstream from the duct exit plane at $75D$.

2.2. *Mean flow measurements*

Axial static pressure gradients were obtained from the wall pressure tappings. Radial static pressure gradients in the curved duct were obtained from the axial pressure gradient data. The static head difference between inner and outer walls was approximately 2% of the mean velocity head, and a linear variation of static pressure across the duct could be assumed with negligible error.

Mean velocities were measured by flattened total-head probes working against the wall static pressure tappings, corrected on the above basis for radial static pressure variation, and the probes were calibrated against an N.P.L.-type substandard Pitot-static tube. Subsidiary mean velocity data obtained during hot-wire anemometer measurements were used as a check on the low velocity data, but were not considered to be sufficiently accurate at higher velocities.

The shear velocity u_τ was obtained by the Clauser-chart method (Clauser 1954), using the universal logarithmic-law constants ($\kappa = 0{\cdot}41$, $A = 5{\cdot}0$) suggested by Coles (1968). Preston tubes were also used with the calibration curves of Patel (1965), and gave estimates within 2% of the Clauser-chart values in all cases. Use of the axial pressure gradient to determine shear velocities was considered to be unreliable, owing to the sensitivity of the method to small mean flow accelerations, but check calculations for the fully developed flow gave good agreement with the mean values derived from the Clauser-chart method.

2.3. *Turbulence measurements*

An unlinearized constant-temperature hot-wire anemometer of the type described in Perry & Morrison (1971*a*) was used, and the dynamic calibration technique given in Perry & Morrison (1971*b*) was adopted to obtain the small-perturbation velocity sensitivity of the whole system directly, without recourse to assumptions of heat-transfer laws, or to curve fitting or numerical differentiation of calibration data. Run data were rejected if recalibration after a run failed to agree with the initial calibration within 2% of sensitivity. Wollaston wire elements 4 μm and 5 μm in diameter and 0·8–1·2 mm long were used for measurements of the streamwise (r.m.s.) intensity $\tilde{u}$. To avoid position errors caused by wire bowing due to thermal expansion, a short-range telescope focused on the active section of the wire and its reflexion in the wall was normally used to determine the wall distance y near the wall. The data were obtained as ensemble averages, over total periods of up to 2 min per point to ensure convergence of the mean, and were corrected for ambient temperature changes only. The total uncertainty in the $\tilde{u}$ data is estimated as $\pm 2\%$.

The transverse r.m.s. turbulence intensities $\tilde{v}$ and $\tilde{w}$ and (kinematic) Reynolds stresses $-\overline{uv}$ and $-\overline{uw}$ were obtained from similar cross-wire techniques, using tungsten wires 5 μm in diameter and 1·2 mm long. The dynamic calibration procedures detailed in Morrison, Perry & Samuel (1972) were used, obviating the need for assumptions of wire angles, matching of wire sensitivities or matching of anemometer channels. The cross-wire technique, however, remains inherently less accurate than the single normal wire procedure for $\tilde{u}$, especially when Reynolds stresses are to be obtained, and the uncertainty in these measurements is estimated as $\pm 5\%$.

Energy spectra for the streamwise component $\overline{u^2}$ were obtained from a proportional-pass-band filter system, set to give a nominal pass-band of $\pm 10\%$ of the centre-frequency over a measurement range of 0·2 Hz to 10 kHz. The pass-band shape was confirmed by measurement to be independent of the centre-frequency. Total sampling times of up to 50 mean periods were necessary to ensure mean convergence in the low frequency data. System offsets were zeroed for each reading and system noise was subtracted to obtain the true levels. The wires were 4 μm in diameter and 0·8–1·2 mm long, and the measured spectra were corrected for wire length effects using the method of Wyngaard (1968).

Further details of the apparatus and techniques are given in Hunt & Joubert (1978), together with a listing of data. A more complete analysis of the straight duct flow is given in Hunt & Joubert (1977).

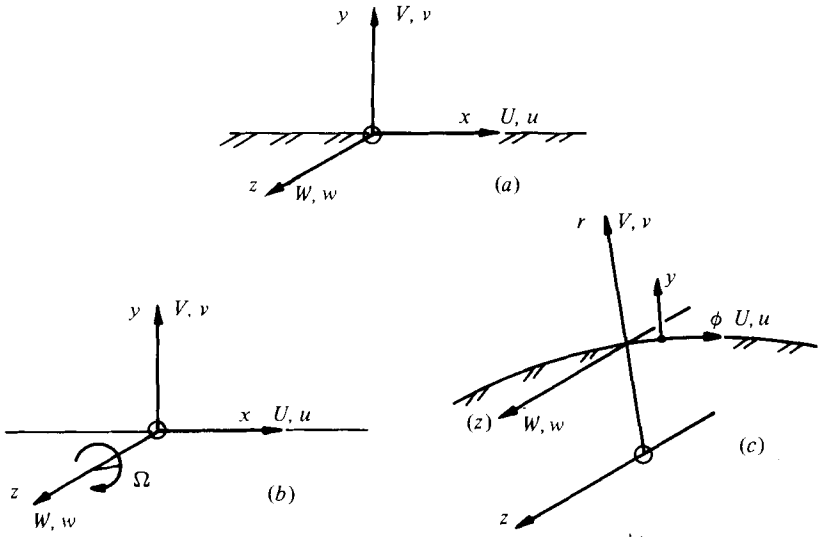

FIGURE 2. Axes and sign conventions. (*a*) Straight stationary duct. (*b*) Straight rotating duct. (*c*) Curved stationary duct.

3. Analysis

It is convenient to examine the hypotheses available for flows with streamline curvature in terms of the basic equations for fully developed, two-dimensional, incompressible steady flow in:

(*a*) a straight stationary smooth-walled duct,

(*b*) a similar straight duct rotating about an axis parallel to its walls and perpendicular to the flow direction,

(*c*) a smooth-walled duct with constant radius of curvature.

The second case provides a useful 'bridge' between the other two. The terminology and sign conventions used here are given in figure 2. The 'left-handed' definition adopted for Ω allows streamline turning rates Ω and U/r to be defined consistently as positive for the stabilized wall flows in both rotating and curved duct flows.

The momentum equations for the streamwise (x, ϕ) direction are

$$0 = -\frac{1}{\rho}\frac{\partial P}{\partial x} + \nu\frac{\partial^2 U}{\partial y^2} - \frac{\partial \overline{uv}}{\partial y}, \tag{1a}$$

$$0 = \left\{-\frac{1}{\rho}\frac{\partial P}{\partial x} + \Omega^2 x\right\} + \nu\frac{\partial^2 U}{\partial y^2} - \frac{\partial \overline{uv}}{\partial y}, \tag{1b}$$

$$0 = -\frac{1}{\rho r}\frac{\partial P}{\partial \phi} + \nu\left(\frac{\partial^2 U}{\partial r^2} + \frac{1}{r}\frac{\partial U}{\partial r} - \frac{U}{r^2}\right) - \frac{\partial \overline{uv}}{\partial r} - \frac{2\overline{uv}}{r}, \tag{1c}$$

The transverse (y, r) momentum equations are

$$0 = -\frac{1}{\rho}\frac{\partial P}{\partial y} - \frac{\partial \overline{v^2}}{\partial y}, \tag{2a}$$

$$0 = \left\{-\frac{1}{\rho}\frac{\partial P}{\partial y} + 2\Omega U\right\} - \frac{\partial \overline{v^2}}{\partial y}, \tag{2b}$$

$$0 = \left\{-\frac{1}{\rho}\frac{\partial P}{\partial r} + \frac{U^2}{r} + \frac{\overline{u^2}}{r}\right\} - \frac{\partial \overline{v^2}}{\partial r} - \frac{\overline{v^2}}{r}. \tag{2c}$$

With the boundary condition $\overline{vw} = 0$ at the wall, the z momentum equations all yield $\overline{vw} = 0$ over the whole flow field.

Following the practice of workers concerned with rotating flows (see, for example, Moon 1964; Halleen & Johnston 1967), the term in braces in (1*b*) may be written as

$$-\frac{1}{\rho}\frac{\partial P}{\partial x} + \Omega^2 x = -\frac{1}{\rho}\frac{\partial}{\partial x}(P - \tfrac{1}{2}\rho\Omega^2 x^2) = -\frac{1}{\rho}\frac{\partial P^*}{\partial x},$$

where $P^* = P - \frac{1}{2}\rho\Omega^2 x^2$ is the 'reduced pressure'. The reduced pressure gradient is then the gradient in excess of that required for equilibrium in the imposed acceleration field, and the term taken as a whole has the same physical significance as the streamwise pressure gradient terms for the other two flows.

The concept may be extended to allow the terms in braces in (2*b*,*c*) to be interpreted as reduced transverse pressure gradients, carrying the same physical significance as the simpler transverse pressure gradient term in (2*a*).

Comparison of (1*a*) with (1*b*), and (2*a*) with (2*b*) shows that streamline rotation has no effect on the form of the viscous or turbulent shear-stress terms, nor on the transverse Reynolds-stress gradient term. The apparent 'extra terms' in the curved flow equations arise from their development as moment of momentum balances for an axisymmetric element, but the straight flow equations can, of course, be developed as limiting cases of the same balances, and no additional or essentially different physical processes are implied by the terms. A particular direct point of comparison is the expression for total kinematic shear stress, which has the common form

$$\begin{aligned}\tau/\rho &= \nu \times (\text{rate of strain of mean flow}) - \overline{uv} \\ &= \begin{cases} \nu\,\partial U/\partial y - \overline{uv} & \text{for the straight flows,} \\ \nu(\partial U/\partial r - U/r) - \overline{uv} & \text{for curved flow.}\end{cases}\end{aligned}$$

The mean flow kinetic energy balance under the present restrictions reverts in each case to the form

$$0 = U \times (\text{streamwise momentum equation}).$$

The extra term $-\overline{uv}\,2U/r$ which occurs in the curved flow equation is then seen to form part of the complete term $Ur^{-2}\,\partial r(-\overline{uv}r)/\partial r$, which is directly comparable to the straight flow term $U\partial(-\overline{uv})/\partial y$, and again no additional physical process is implied. The mean flow equations for all three cases are then essentially identical, and offer little guidance to a mechanism by which streamline curvature or rotation can have their marked effects on turbulent duct flow.

Various attempts have been made to predict mean velocity profiles in curved flows from the momentum considerations, but they have had limited success. The classical Prandtl (1931) extension of his mixing-length argument significantly underestimates the effect of curvature on wall-region flow, and Bradshaw (1969) found that his generalization of the theory could not give an adequate representation of the profile (in this case for the rotating-duct data of Halleen & Johnston 1967). Rotta (1967) used a mixing-length approach to obtain a deviation from the normal straight-wall logarithmic law, parametric in the wall radius Reynolds number $r_w u_\tau/\nu$, but again this significantly underestimates the effect of curvature.

Predictions of the central-region mean flow have been based on Taylor's (1935) extension of the vorticity transport theory, and on von Kármán's (1951) extension of the 'mechanical similitude' concept (see, for example, Wattendorf 1935; Marris 1956, 1960; Kinney 1967; Ellis & Joubert 1974). The predictions at best give limited correlation only, and this is restricted to highly curved flows. Probably the most successful was Wattendorf's proposal of an angular-momentum defect equation in the form

$$\frac{K_1 - Ur}{r\left(-\frac{1}{\rho}\frac{\partial P}{r_p \partial \phi} b_p\right)^{\frac{1}{2}}} \quad \text{or} \quad \frac{U_p - U}{\left(-\frac{1}{\rho}\frac{\partial P}{r_p \partial \phi} b_p\right)^{\frac{1}{2}}} \quad \text{as a function of} \quad \frac{y}{b_p}, \tag{3}$$

where r_p is the radius at which $Ur = K_1$, the maximum value, b_p is the distance from this radius to the wall, and U_p is the 'potential velocity' as used by later investigators ($U_p r = K_1$). This is found to give coincidence of central-region data from both inner and outer walls of highly curved flows (see also Yeh, Rose & Lien 1956), but the profile obtained varies in shape as the duct curvature alters, and differs from the limiting straight-wall profile shape.

More recent proposals have been based on the turbulence energy and turbulent shear-stress correlation equations. In contrast to the mean flow equations, these equations include terms representing identifiable additional physical processes due to streamline curvature or rotation. Under the present restrictions, the equations for the three flows take the following forms: for the streamwise component u,

$$0 = -\frac{\overline{u}}{\rho}\frac{\overline{\partial p}}{\partial x} - \frac{1}{2}\frac{\overline{\partial u^2 v}}{\partial y} + \nu\overline{u\nabla^2 u} - \overline{uv}\frac{\partial U}{\partial y}, \tag{4a}$$

$$0 = -\frac{\overline{u}}{\rho}\frac{\overline{\partial p}}{\partial x} - \frac{1}{2}\frac{\partial \overline{u^2 v}}{\partial y} + \nu\overline{u\nabla^2 u} - \overline{uv}\frac{\partial U}{\partial y} - \overline{uv}\,2\Omega, \tag{4b}$$

$$0 = -\frac{\overline{u}}{\rho}\frac{\overline{\partial p}}{r\partial \phi} - \frac{1}{2r}\frac{\partial \overline{r u^2 v}}{\partial r} + \nu\left(\overline{u\nabla^2 u} - \frac{\overline{u^2}}{r} + \frac{2}{r}\frac{\overline{u}}{r}\frac{\overline{\partial v}}{\partial \phi}\right) - \overline{uv}\left(\frac{\partial U}{\partial r} - \frac{U}{r}\right) - \overline{uv}\frac{2U}{r} - \frac{\overline{u^2 v}}{r}; \tag{4c}$$

for the transverse component v,

$$0 = -\frac{\overline{v}}{\rho}\frac{\overline{\partial p}}{\partial y} - \frac{1}{2}\frac{\overline{\partial v^3}}{\partial y} + \nu\overline{v\nabla^2 v}, \tag{5a}$$

$$0 = -\frac{\overline{v}}{\rho}\frac{\overline{\partial p}}{\partial y} - \frac{1}{2}\frac{\overline{\partial v^3}}{\partial y} + \nu\overline{v\nabla^2 v} + 0 + \overline{uv}\,2\Omega, \tag{5b}$$

$$0 = -\frac{\overline{v}}{\rho}\frac{\overline{\partial p}}{\partial r} - \frac{1}{2}\frac{1}{r}\frac{\partial \overline{r v^3}}{\partial r} + \nu\left(\overline{v\nabla^2 v} - \frac{\overline{v^2}}{r} - \frac{2}{r}\frac{\overline{v}}{r}\frac{\overline{\partial u}}{\partial \phi}\right) + 0 + \overline{uv}\frac{2U}{r} + \frac{\overline{u^2 v}}{r}; \tag{5c}$$

for the transverse component w,

$$0 = -\frac{\overline{w}}{\rho}\frac{\overline{\partial p}}{\partial z} - \frac{1}{2}\frac{\partial \overline{v w^2}}{\partial y} + \nu\overline{w\nabla^2 w}, \tag{6a,b}$$

$$0 = -\frac{\overline{w}}{\rho}\frac{\overline{\partial p}}{\partial z} - \frac{1}{2}\frac{1}{r}\frac{\partial \overline{r v w^2}}{\partial r} + \nu\overline{w\nabla^2 w}. \tag{6c}$$

Summation of (4), (5) and (6) for each flow gives the equations for the total turbulence energy $\frac{1}{2}\overline{q^2} = \frac{1}{2}(\overline{u^2}+\overline{v^2}+\overline{w^2})$:

$$0 = -\frac{1}{\rho}\frac{\partial \overline{pv}}{\partial y} - \frac{1}{2}\frac{\partial}{\partial y}\overline{vq^2} + \nu\left(\overline{u\nabla^2 u} + \overline{v\nabla^2 v} + \overline{w\nabla^2 w}\right) - \overline{uv}\frac{\partial U}{\partial y}, \tag{7a,b}$$

$$0 = -\frac{1}{\rho}\frac{1}{r}\frac{\partial \overline{rpv}}{\partial r} - \frac{1}{2}\frac{1}{r}\frac{\partial \overline{rvq^2}}{\partial r} + \nu\left(\overline{u\nabla^2 u} + \overline{v\nabla^2 v} + \overline{w\nabla^2 w} - \frac{(\overline{u^2}+\overline{v^2})}{r^2} + \frac{2}{r}\left(\overline{u\frac{\partial v}{r\,\partial\phi}} - \overline{v\frac{\partial u}{r\,\partial\phi}}\right)\right) - \overline{uv}\left(\frac{\partial U}{\partial r} - \frac{U}{r}\right). \tag{7c}$$

The equation for the turbulent kinematic shear stress (Reynolds stress) $-\overline{uv}$ are

$$0 = \frac{1}{\rho}\left(\overline{u\frac{\partial p}{\partial y}} + \overline{v\frac{\partial p}{\partial x}}\right) + \frac{\partial \overline{uv^2}}{\partial y} - \nu(\overline{u\nabla^2 v} + \overline{v\nabla^2 u}) + \overline{v^2}\frac{\partial U}{\partial y}, \tag{8a}$$

$$0 = \frac{1}{\rho}\left(\overline{u\frac{\partial p}{\partial y}} + \overline{v\frac{\partial p}{\partial x}}\right) + \frac{\partial \overline{uv^2}}{\partial y} - \nu(\overline{u\nabla^2 v} + \overline{v\nabla^2 u}) + \overline{v^2}\frac{\partial U}{\partial y} - (\overline{u^2}-\overline{v^2})\,2\Omega, \tag{8b}$$

$$0 = \frac{1}{\rho}\left(\overline{u\frac{\partial p}{\partial r}} + \overline{v\frac{\partial p}{r\,\partial\phi}}\right) + \frac{1}{r}\frac{\partial r\overline{uv^2}}{\partial r} - \nu\left(\overline{u\nabla^2 v} + \overline{v\nabla^2 u} - \frac{2\overline{uv}}{r^2}\right) + \overline{v^2}\left(\frac{\partial U}{\partial r} - \frac{U}{r}\right) - (\overline{u^2}-\overline{v^2})\frac{2U}{r} - \frac{\overline{u(u^2-v^2)}}{r}. \tag{8c}$$

Following Townsend (1956) and Hinze (1959), the physical significance of the first four terms in each equation may be given as follows:

First term = the transport of turbulent energy by fluctuating pressure gradients.

Second term = the diffusion of energy by fluctuating transverse velocity gradients.

Third term = dissipation and diffusion of energy by viscous stresses.

Fourth term = production of turbulence energy, i.e. extraction of energy from the mean flow, by the interaction of turbulent shear stresses with the rate of strain of the mean flow. The form of this term is (turbulent shear stress × rate of strain of mean flow) in each case.

The terms in the shear stress equations have corresponding meanings.

The interpretation of the final terms is less well agreed upon. For (4) and (5) the terms are $\pm\overline{uv}\times 2\Omega$ and $\pm\overline{uv}\times 2U/r$, where the (small) triple velocity correlation is ignored here for convenience. They are commonly treated as additional 'production' terms, see, for example, Bradshaw (1969, 1973) and Eskinazi & Yeh (1956), where 2Ω and $2U/r$ are viewed as extra rates of strain of the mean flow, and the terms are added to the fourth terms of their equations.

The total 'production' terms for the streamwise component u then become

$$-\overline{uv}(\partial U/\partial y + 2\Omega)$$

in (4*b*) and

$$-\overline{uv}(\partial U/\partial r + U/r)$$

in (4*c*), i.e. of the form (turbulent shear stress) × (vorticity of mean flow relative to stationary axes).

'Production' terms then also appear for the transverse component v, $+\overline{uv}\times 2\Omega$ in

(5*b*) and $+\overline{uv} \times 2U/r$ in (5*c*). For $\overline{uv}$ negative, i.e. positive shear stress, and Ω or U/r positive the interpretation entails the concept of 'negative production', implying the reordering of the random fluctuating velocities so that they return energy to the mean flow, at the same rate as the (presumably normal) extra positive production removes energy from the mean flow. Eskinazi & Erian (1969) give a discussion of this phenomenon, and adduce some evidence for its existence, but the physical flow mechanism which would give negative production remains obscure.

The terms arise from the need to include Coriolis forces in the analyses, when axes rotating relative to an inertial frame are chosen. Batchelor (1967, § 7.6) notes that 'The Coriolis force... is a deflecting force which does no work on a material element'. The conservative nature of the Coriolis force terms, as distinct from the non-conservative fourth terms (production terms), is of course illustrated by their absence from the equations (7) for the total turbulence energy.

Batchelor's discussion and that of Traugott and Yeh (Traugott 1958) support the interpretation of the final, 'Coriolis' terms in (4) and (5) as representing a conservative reorientation, or transfer of energy from the streamwise direction (x, ϕ) to the transverse direction (y, r), or *vice versa* depending on the signs of Ω or U/r and $\overline{uv}$. Under this interpretation, turbulence energy is produced by the mean flow strain rate on the streamwise component u alone in all three flows; fluctuating pressure and velocity gradients redistribute the energy to the other components and viscous stresses diffuse and dissipate the energy in the same way. The additional effect of streamline curvature or rotation is then to produce an 'energy pump' effect by which some of the existing energy is transferred without loss between the components in the plane of streamline curvature.

Equations (8) for the shear stress $-\overline{uv}$ yield extra terms $-(\overline{u^2}-\overline{v^2}) \times 2\Omega$ in addition to the straight stationary (wall) flow term $-\overline{v^2}\,\partial U/\partial y$, for straight rotating flow, and similar terms for the curved flow.

Here, for positive rotation Ω (or U/r for curved flow), a positive fluctuation u gives rise to a positive acceleration in the v direction and *vice versa*, so the existence of streamwise energy $\overline{u^2}$ leads to a positive change in the $\overline{uv}$ correlation, i.e. a negative change in the shear stress $-\overline{uv}$. Conversely, a positive transverse fluctuation v gives rise to a negative acceleration in the u direction, and *vice versa*, so the existence of transverse energy $\overline{v^2}$ leads to a negative contribution to $\overline{uv}$, i.e. a positive change in shear stress $-\overline{uv}$. Unless $\overline{u^2} = \overline{v^2}$, the net effect is to introduce a highly structured component into the $-\overline{uv}$ correlation.

If $\overline{u^2} > \overline{v^2}$, which is the case in duct flows, especially near the walls (see, for example, Comte-Bellot 1963; Laufer 1950; Eskinazi & Yeh 1956), positive rotation Ω or U/r gives a negative net change in the rate of production of the shear-stress correlation $-\overline{uv}$. Also, in a region in which the shear stress $-\overline{uv}$ is positive, positive rotation or curvature leads to a transfer of energy from $\overline{v^2}$ to $\overline{u^2}$, tending to increase the difference between them and so make the negative change in $-\overline{uv}$ larger.

The fractional change in $-\overline{uv}$ for small values of rotation or curvature may then be large, and the mechanism described appears capable of accounting for the major differences between straight and curved or rotating flows, without the need to propose the existence of special, additional 'production' and 'negative production' processes.

Bradshaw (1969, 1972, 1973) pointed out the analogy between streamline curvature and buoyancy, and by reference to meteorological practice obtained an equation

$$\frac{L}{L_0} = 1+\beta N_{Ri} \approx 1+\gamma \frac{(U/r \text{ or } \Omega)}{\partial U/\partial y} \quad \text{for} \quad N_{Ri} \quad \text{small}. \tag{9a}$$

Here β and γ are constants initially estimated from meteorological data, and N_{Ri} represents the curved and rotating flow analogues of the 'gradient', 'flux' and 'stress' Richardson numbers relating corresponding streamwise and transverse quantities in buoyant flows. L and L_0 are the curved or rotating and straight, stationary flow values respectively of the dissipation length parameter used in Bradshaw, Ferriss & Atwell's (1967) boundary-layer calculation method. In his comprehensive review paper (1973) Bradshaw notes that $\gamma \doteqdot 10$ is required to fit data for curved and rotating flows at small N_{Ri}, implying that the shear-stress distribution is an order of magnitude more sensitive to these effects than was predicted by Prandtl. He recommends specifically that

$$\gamma = \left\{ \begin{matrix} 14 & \text{for corvex wall boundary layers,} \\ 9 & \text{for concave wall boundary layers.} \end{matrix} \right\} \tag{9b}$$

If γ is taken to be the ratio of the extra shear-stress 'production' terms, in (8*b*) and (8*c*), to the production term in straight stationary wall flow, $\overline{v^2}\,\partial U/\partial y$ in (8*a*), then

$$\gamma = 2(\overline{u^2}/\overline{v^2}-1). \tag{10}$$

Wall region data for straight ducts (see, for example, Comte-Bellot 1963) show that $\overline{u^2}/\overline{v^2}$ is ≈ 5 in the logarithmic region, and higher near the position of maximum turbulence energy production. Equation (10) then gives $\gamma = 8$ as a low estimate, and it appears that as a first approximation Bradshaw's arbitrary constant γ can be obtained from straight stationary wall turbulence data. The proposal can be carried further in terms of the 'feedback' effect of the energy transfer term discussed earlier, and yields second-order estimates of γ of similar size and ratio to those given in (9*b*). The present interpretation of the processes represented then appears to provide a direct line of support for Bradshaw's model. Irwin & Smith (1975) include a form of small curvature correction in their calculation method, and find the eddy viscosity then derived from a detailed modelling of energy and shear-stress equation terms to be strongly dependent on curvature. The models are, however, limited by the inevitable defects of the mixing length and eddy viscosity approaches, most importantly that of determining parameters as a function of a single location in the flow, and the precise form of the modelled terms cannot be expected to have general validity. A more general approach perhaps based on regional definitions of the 'active' and 'inactive' parameters in the two-component turbulence model described by Townsend (1961) appears preferable, but no recent attempts are known to the authors.

4. Results and discussion

4.1. *Mean flow*

The flows were investigated for three principal Reynolds numbers: $R_N = DU_m/\nu$ = 30000, 60000 and 130000, where D = duct width, U_m = maximum velocity and ν = kinematic viscosity.

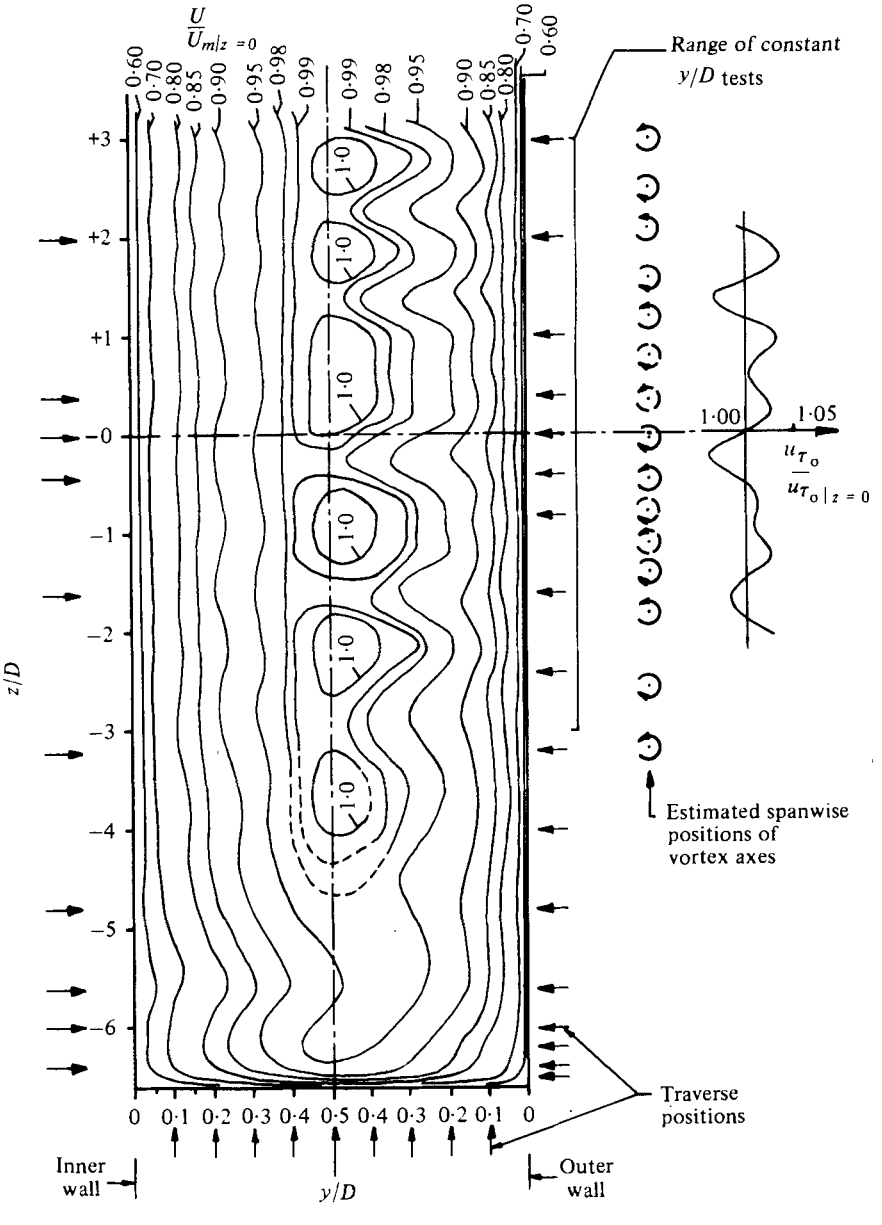

(*a*)

FIGURE 3 (*a*). For legend see next page.

Flow symmetry checks indicated small variations in the velocity profile in the central flow region of the curved duct, and a more extensive investigation of the mean flow profile over the whole duct exit cross-section was carried out for $R_N = 60\,000$. The data for figure 3 (*a*) were obtained as a series of traverses at constant y/D and at constant z/D, at the positions indicated. Interpolation then gave lines of constant velocity ratio, and revealed the cellular structure shown.

The data were taken on four separate occasions, and were taken in a deliberately

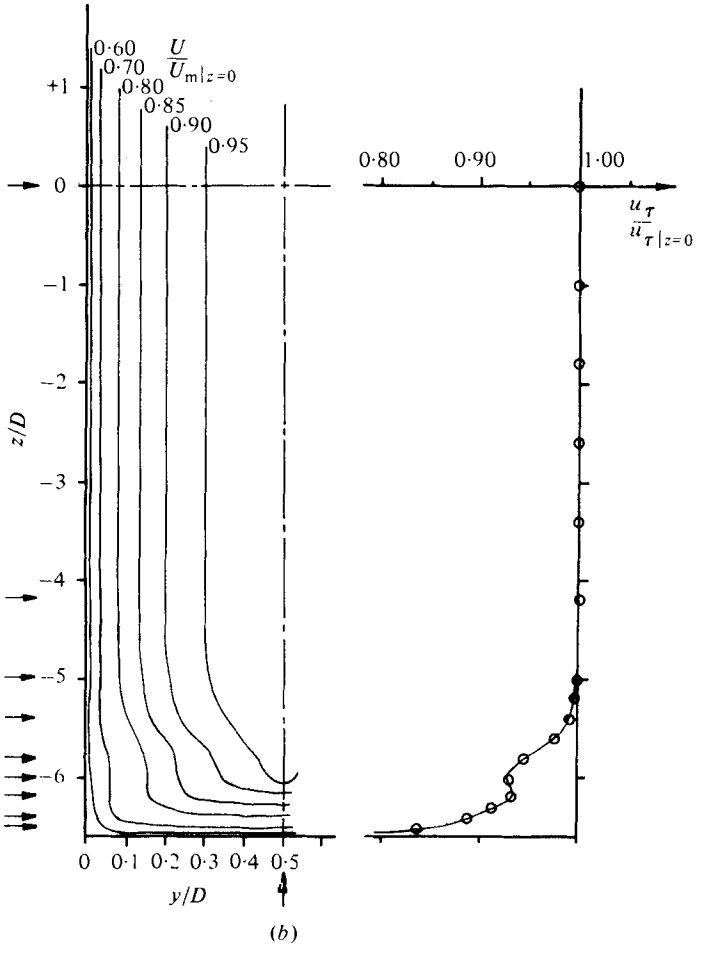

FIGURE 3. Mean flow at (*a*) curved and (*b*) straight duct exit plane, R_N = 60000. Scale change × 4 between horizontal and vertical axes.

non-regular order so that the effects of possible small periodic variations in external parameters such as the tunnel reference head could be readily distinguished from the real variation in the flow pattern. The structure appeared to be stable in its position relative to the duct walls; the small inconsistencies remaining in the data occurred without a regular pattern, and could not be attributed to a spanwise shifting of the structure.

The results for the straight duct, obtained from a similar series of tests, are shown for comparison in figure 3(*b*). The end-wall vortex systems in the curved duct appear to fix the position of the central region structure although Patel (1968) found the cross-flow structure on the central region of his curved boundary layers to be independent of end-wall conditions. Meroney & Bradshaw (1975) also remark on the positional stability of the spanwise structure found in their concave-wall boundary layer, and consider it to be a response to fixed upstream disturbances.

The structure may be interpreted as being due to an array of Taylor–Goertler vortices in the outer part of the central flow; the estimated spanwise positions of the

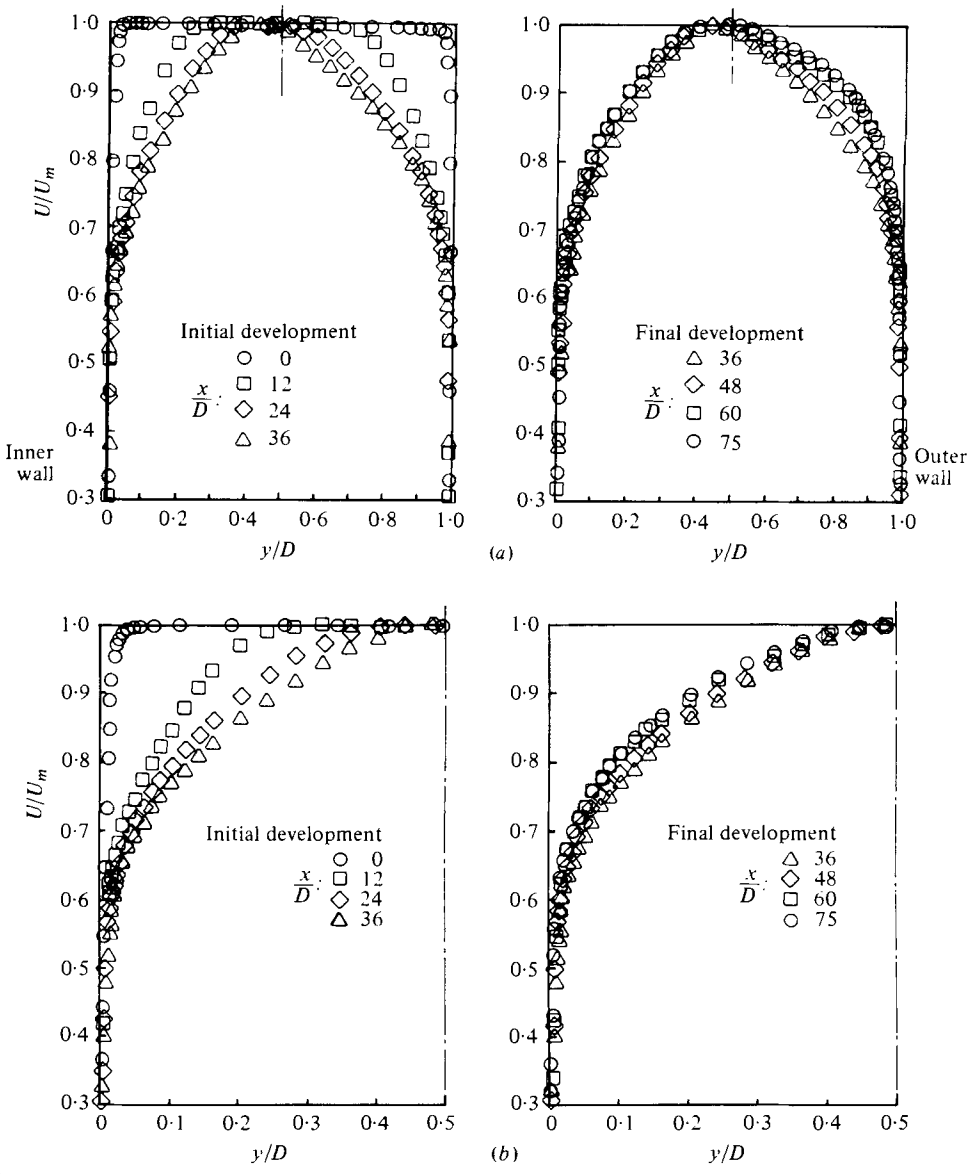

FIGURE 4. Mean flow development in (*a*) curved and (*b*) straight duct: $z/D = 0$, $R_N = 60\,000$.

vortices and their senses of rotation are shown in the figure. The mean spacing of vortex axes in the outer flow $0{\cdot}44D$, but closer inspection leads to the interpretation of the pattern as being due to an array of comparatively strong vortex pairs at $0{\cdot}40D$ spacing, with $1{\cdot}45D$ mean spacing between successive pairs, and with weaker, secondary vortex pairs in the intervening spaces. The variation of the Preston tube measurements of shear velocity indicate the effects of this structure on the flow very near the outer wall.

The deviations of the contours in the inner flow region are consistent with the existence of a weak circulating cross-flow driven by the outer-flow vortex array; the wavelength of the deviations is nearly uniform, with $1{\cdot}42D$ the average value for

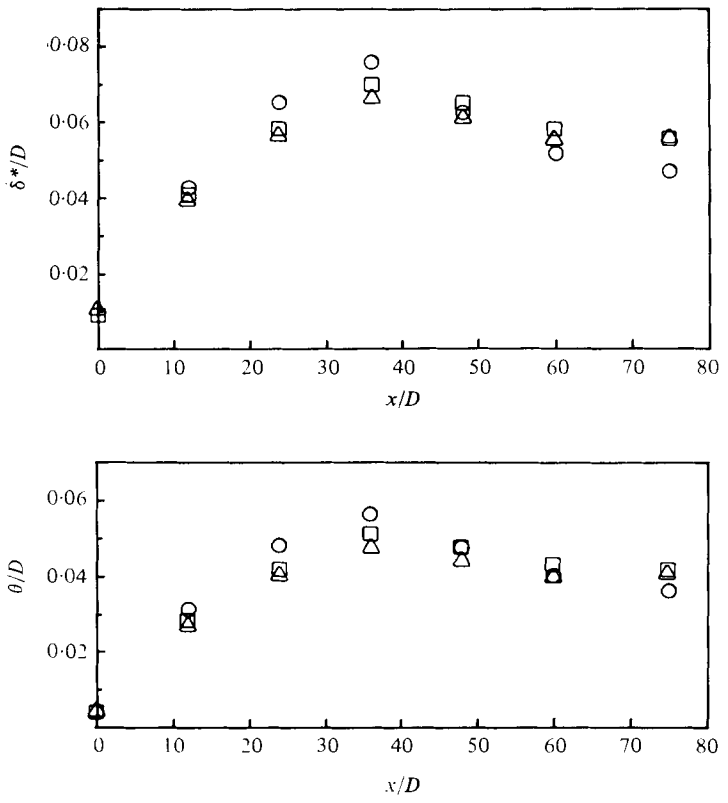

FIGURE 5. Variation of displacement thickness δ^* and momentum thickness θ, $R_N = 60000$. ○, outer wall; △, inner wall; □, straight wall.

$z/D < +2$, and the amplitudes of deviations in the inner region are much less than the comparable outer-region amplitudes. Minimum deviation amplitudes occur for $y_i/D = 0{\cdot}38$ (where y_i is distance from the inner wall), which may be taken as indicating near-zero cross-flow velocity V at this surface. This implies a distinct separation between outer and inner flows similar to that obtained by Taylor (1923) for viscous flow between rotating cylinders, but the assumed cross-flow senses within the regions are not compatible with this model. However, the major part of the recirculating flow does appear to be confined to the outer region.

Following the discussion by So & Mellor (1975) of the vortex stability work of Smith (1955) and Tani (1962), the present data give a turbulent Goertler number $G_T = 0{\cdot}87$, a vortex spacing parameter $a\theta = 0{\cdot}57$ and a curvature parameter $a\bar{r} = 1430$, where the outer wall momentum thickness θ and overall mean vortex spacing $0{\cdot}44D = 2\pi/a$ have been used. The flow is then predicted to be marginally stable, but the data point falls in the same proximity to the stability boundary as those of Tani for a flow observed to be marginally unstable, similar to the present case.

The flow-visualization studies of rotating duct flow reported in Halleen & Johnston (1967), Lezius & Johnston (1971) and Johnston, Halleen & Lezius (1972) gave clear evidence of the existence of Taylor–Goertler vortex systems. In the second study, a flow stability analysis gave a small lower limit of the rotation parameter for the existence of the vortex pattern. In their tests, the experimenters were careful to

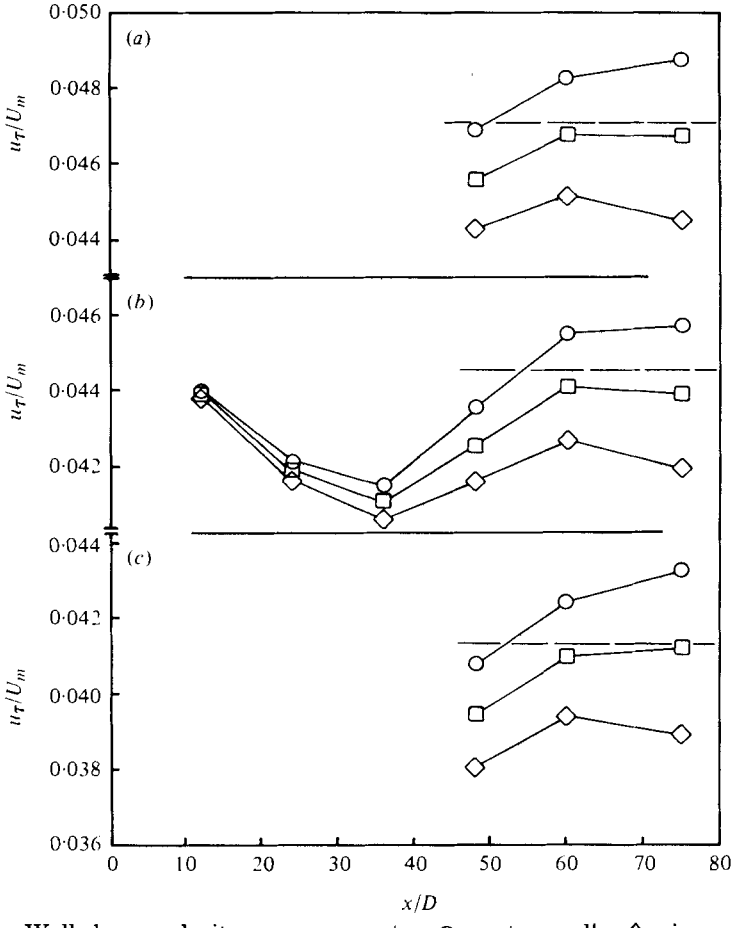

FIGURE 6. Wall-shear velocity measurements. ○, outer wall; ◇, inner wall; □, mean, from shear stresses; ---, mean, from pressure gradient. (*a*) R_N = 30000. (*b*) R_N = 60000. (*c*) R_N = 130000.

distinguish the vortex pattern from end-wall induced secondary flows and from wall flow structures of the types described by Kline *et al.* (1967), Kim, Kline & Reynolds (1971) and others (these structures were also observed in the rotating duct flow), and the existence of vortex systems when the rotation parameter exceeds a specifiable minimum value seems well confirmed. The specific stability limit given by Lezius & Johnston was $R_0 = \Omega D/\overline{U} = 0{\cdot}022$, where $\overline{U}$ is the bulk mean velocity. When the present correspondence of terms is applied, the mean streamline turning rate $\overline{U}/\bar{r}$ may be proposed to replace Ω, and the analogous curved flow parameter becomes simply $D/\bar{r}$, equal to 0·01 in the present case. The existence of the vortex structure then indicates that, if the analogy holds in these broad terms for stability determinants, curved duct flow is significantly less stable than rotating straight duct flow.

The rest of the data were taken in the centre-line plane of the ducts, $z/D = 0$. Figure 3(*a*) indicates that spanwise gradients due to the secondary flow were near maximum at this position, and the good repeatability found for the data provides further

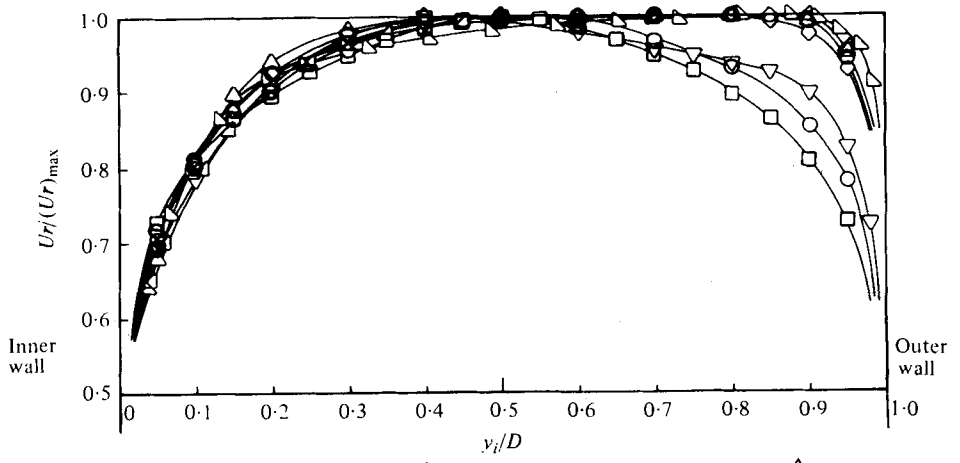

FIGURE 7. Angular momentum profiles. ◺, Yeh *et al.* (1956), $r_o/r_i = 1{\cdot}33$; ⬡, Wattendorf (1935), channel II, $r_o/r_i = 1{\cdot}25$; △, Ellis & Joubert (1974), 15 in. channel, $r_o/r_i = 1{\cdot}17$; ◿, Eskinazi & Yeh (1956), $r_o/r_i = 1{\cdot}11$; ◇, Wattendorf (1935), channel I, $r_o/r_i = 1{\cdot}11$; ▽, Ellis & Joubert (1974), 75 in. channels, $r_o/r_i = 1{\cdot}03$; ○, present curved duct, $r_o/r_i = 1{\cdot}01$; □, present straight duct, $r_o/r_i = 1{\cdot}00$.

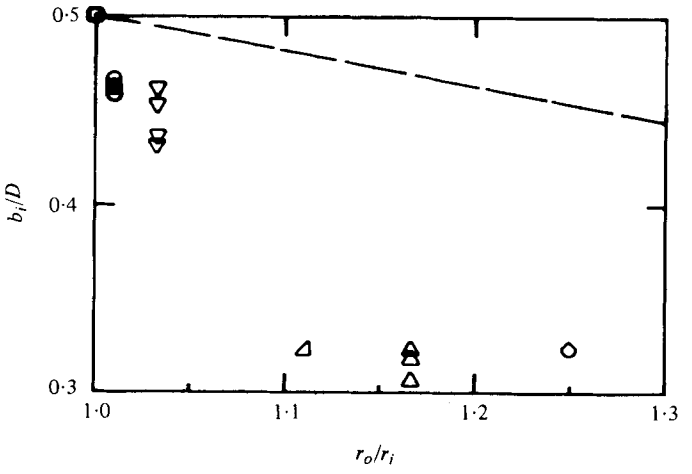

FIGURE 8. Position of surface zero shear stress, Symbols as in figure 7. ---, laminar flow relation.

confirmation of the positional stability of the central flow structure. The small inconsistencies remaining in some of the curved flow data were probably due to small errors in setting traverse position, rather than shifting of the flow structure.

The development of the mean velocity profile for each duct is shown for one Reynolds number in figures 4 (*a*) and (*b*). The evolution of the final profile shape for the present small curvature follows a very similar pattern to that for the straight flow. Figure 5 gives a comparison of displacement thickness δ^* and momentum thickness for the developing flows. Figure 6 shows the variation of the inner and outer wall shear velocities u_{τ_i} and u_{τ_o} with streamwise position and Reynolds number, and compares the independent estimates of the mean shear velocity, defined by $\bar{u}_\tau = [(u_{\tau_i}^2 r_i^2 + u_{\tau_o}^2 r_o^2)/2\bar{r}^2]^{\frac{1}{2}}$ from moment equilibrium requirements, where r_i, r_o and $\bar{r}$ are the inner, outer

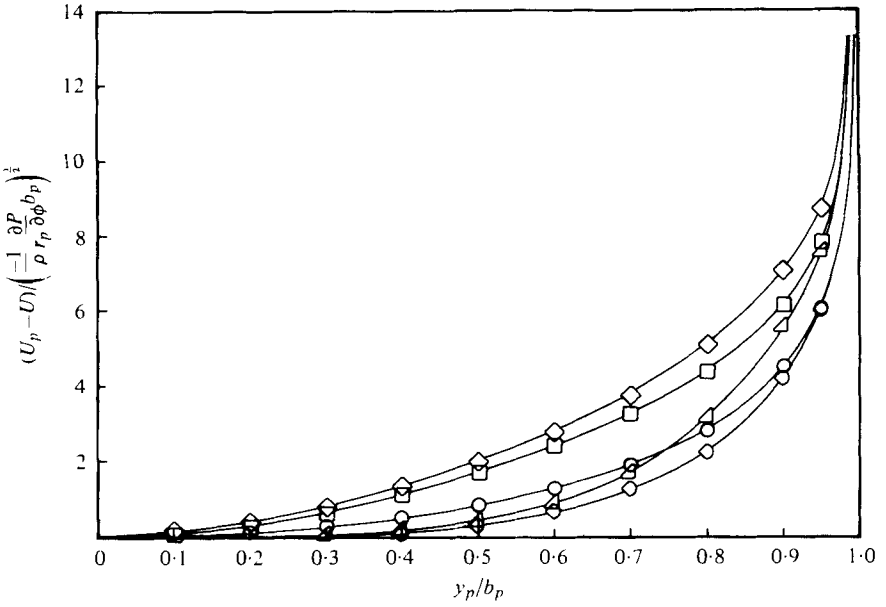

FIGURE 9. Similarity proposal of Wattendorf (1935). ◇, Wattendorf (1935), inner and outer walls; △, Eskinazi & Yeh (1956), inner and outer walls; ◇, present inner-wall data; ○, present outer-wall data; □, present straight-wall data.

and mean wall radii respectively, and $\overline{u}_\tau = (-D/2\rho \times \partial P/\bar{r}\,\partial\phi)^{\frac{1}{2}}$ from the measured static pressure gradients.

The upstream flow outside the boundary layers was irrotational, but the present flow shows no marked tendency to assume an irrotational profile (Ur = constant) at full development, which was a characteristic of most of the earlier, more highly curved flows investigated. Figure 7 illustrates this by comparing the angular momentum profiles obtained. Figure 8 shows the corresponding data, where available, for the position of the surface of zero shear stress, where b_i is the radial distance between the inner wall and the surface of zero shear stress. For the present data, b_i was obtained from the wall shear velocity measurements, using a linear approximation to the total shear-stress distribution. For the duct curvature used here the approximation gives negligible error, and the procedure is much more accurate than either the use of cross-wire measurement to locate $-\overline{uv} = 0$ or estimation of the point of zero strain rate $\partial U/\partial r - U/r = 0$ from the mean velocity profiles.

Figures 7 and 8 demonstrate the possibility of distinguishing between 'inertia-dominated' and 'shear-dominated' classes of curved duct flows, and the need for the distinction. The 'inertia-dominated' flows are characterized by a near-irrotational mean velocity profile at full development, and share a common geometric position of the surface of zero shear stress relative to the duct walls. The 'shear-dominated' flows exhibit no significant regions of irrotational flow, and their position of zero shear stress is strongly dependent on the degree of curvature of the flow; Wattendorf's (1935) similarity proposal (3) may assist in the distinction. Figure 9 gives a comparison of the present data for straight and curved flows (within the 'shear-dominated' class) with the mean flow data from the experiments of Wattendorf and Eskinazi & Yeh (1956) (in the 'inertia-

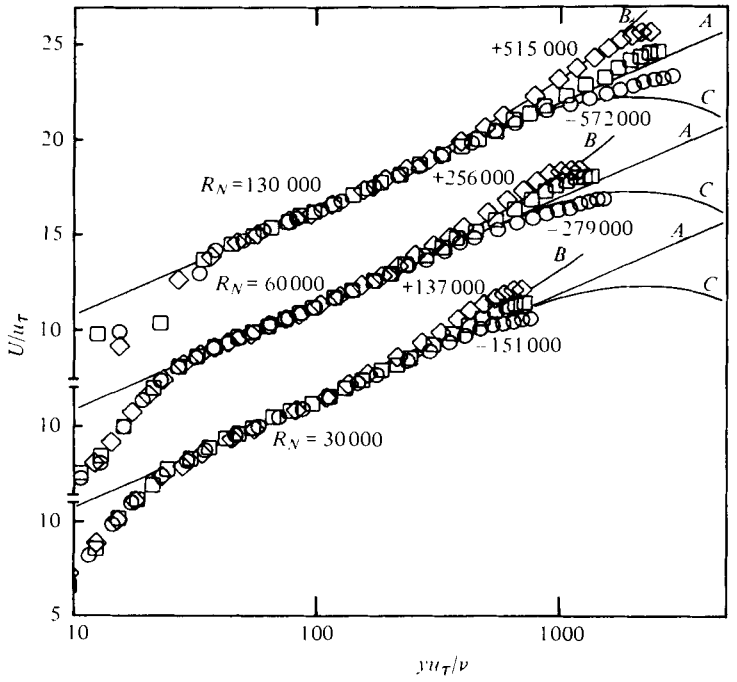

FIGURE 10. Mean velocity profiles in wall-law co-ordinates. $x/D = 75$. *A*, $U/u_\tau = 1/0{\cdot}41 \times \ln yu_\tau/\nu + 5{\cdot}0$ (Coles 1968); *B*, $r_w u_\tau/\nu = +20\,000$ (Rotta 1967); *C*, $r_w u_\tau/\nu = -20\,000$ (Rotta). Present values of $r_w u_\tau/\nu$ are as shown.

dominated' class). The differences between the proposed classes of curved flow are clear.

Direct comparison of the wall-region mean flow data for the present three wall curvature cases is made in figure 10, where the conventional (straight) wall-similarity co-ordinates are used. In this and all subsequent figures, the shear velocity used is that for the adjacent wall. A constant wall-distance correction of $0{\cdot}15 \times$ probe height has been applied to all data, following the procedures of Patel & Head (1969). Representative curves from Rotta's (1967) paper are also given, and their relation to the present data is similar to that found by previous workers.

The common logarithmic region is to some extent a product of the Clauser-chart technique by which the shear velocities were determined, but figure 6 demonstrates independent support for the estimates. The common region of the profiles extends closer to the wall than the logarithmic region, and the differences between profiles are confined to the central flow region.

The result may be argued to be simply due to the very slight curvature used here. The ratio

$$\frac{U/r}{\partial U/\partial y}$$

in the logarithmic region of the present curved-wall flows is of the order of 1/100, so that even if the wall-region mean velocity profile was directly affected by curvature, the effect in the present case would be negligible.

The conventional wall-similarity hypothesis does, however, appear to be applicable directly to wall flows with small curvature. Recent workers have proposed modifica-

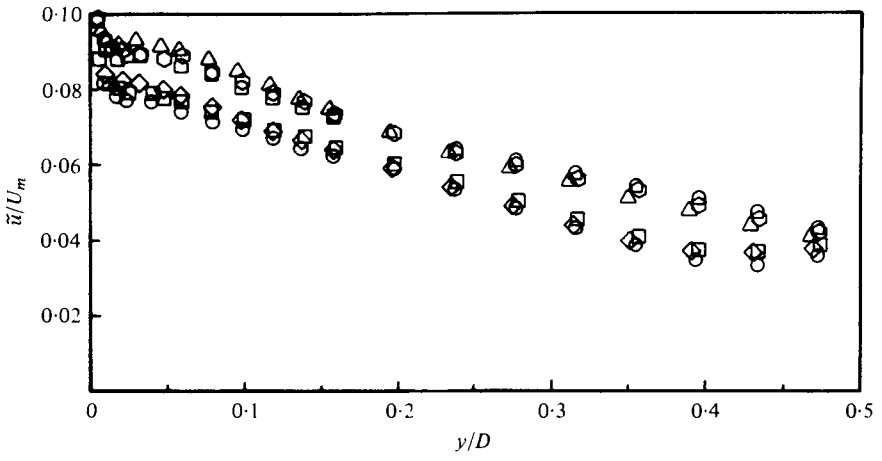

FIGURE 11. Development of streamwise turbulence intensity, $R_N = 130000$. Inner wall: ○, $x/D = 48$; □, $x/D = 60$; ◇, $x/D = 75$. Outer wall: ⌂, $x/D = 49$; ⬯, $x/D = 60$; △, $x/D = 75$.

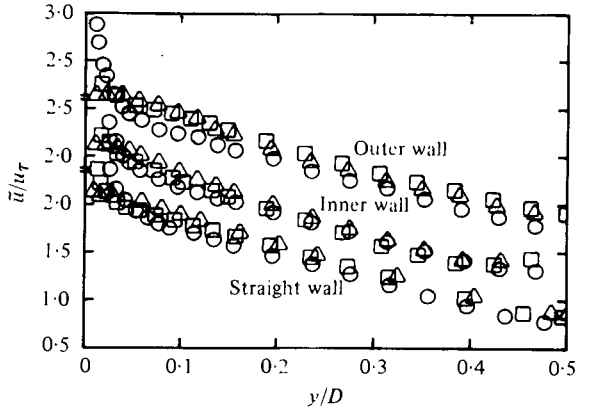

FIGURE 12. Streamwise turbulence intensity in the central region, $x/D = 75$. ○, $R_N = 30000$; □, $R_N = 60000$; △, $R_N = 130000$.

tions to the hypothesis (see, for example, Meroney & Bradshaw 1975), and the data for the highly curved, 'inertia-dominated' flow of Ellis & Joubert (1974) indicates significant curvature effects at positions well inside the corresponding straight-wall logarithmic mean flow regions.

4.2. *Turbulence intensities*

The development of the streamwise r.m.s. turbulence intensity $\tilde{u}$ at the downstream end of the duct is shown for the highest Reynolds number in figure 11. The discrepancies between levels measured at the final two stations are reasonably small, and the turbulence structure is considered to have been very nearly fully developed at the final station at this Reynolds number. Turbulence structure development at the two lower Reynolds numbers is then taken to have been practically complete. The discrepancies are similar to those of the mean velocity profile, which was fully developed

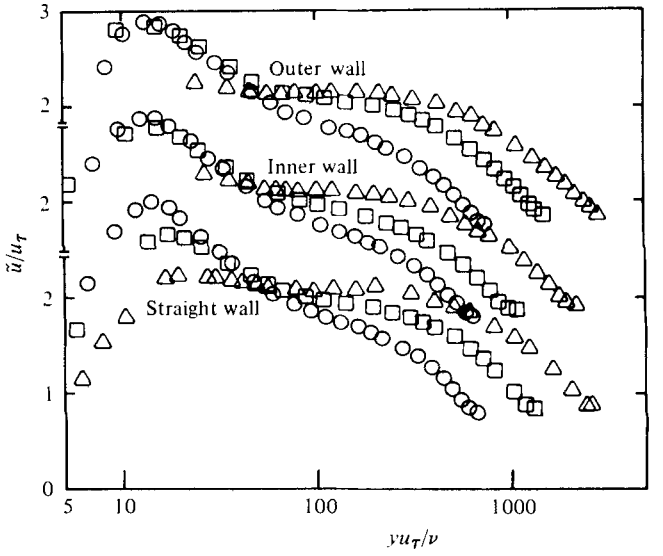

FIGURE 13. Streamwise turbulence intensity in the wall region, $x/D = 75$. Symbols as in figure 12.

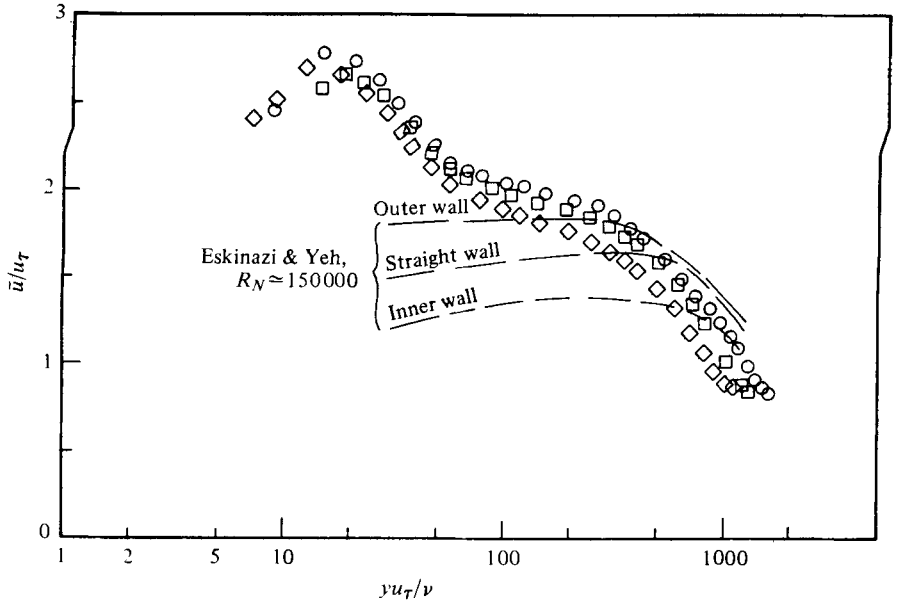

FIGURE 14. Comparison of streamwise turbulence intensities for inner-, outer- and straight-wall flows, $R_N = 60000$. ○, outer wall; ◇, inner wall; □, straight wall.

to a similar degree of certainty. The axial positions $x/D = 60$, 75 used here may be compared with Comte-Bellot's result of a length of $60D$ being required for full development of her straight duct mean flow and turbulence structure, at more than twice the present maximum Reynolds number.

The figure also permits a direct comparison of absolute turbulence intensities in the inner and outer regions of the central flow, and it is seen that the difference

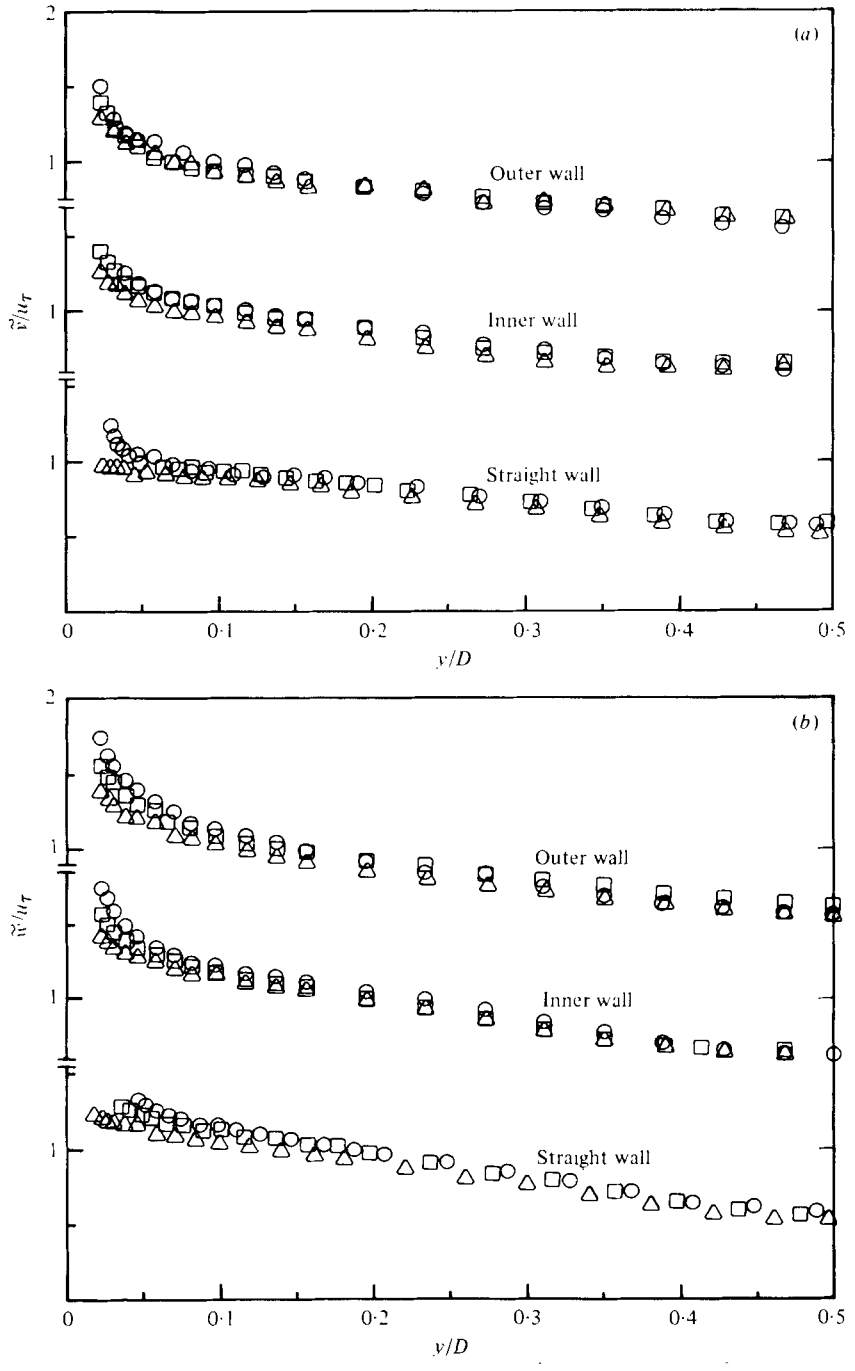

FIGURE 15. Transverse turbulence intensities in the central region, $x/D = 75$. (*a*) Component in y, r direction. (*b*) Component in z direction. ○, $R_N = 30000$; □, $R_N = 60000$; △, $R_N = 130000$.

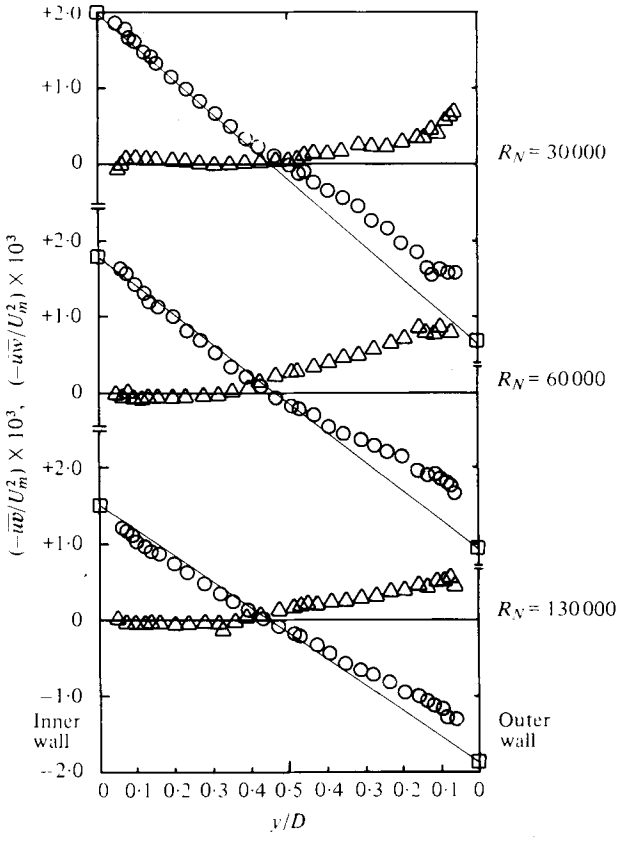

FIGURE 16. Measured Reynolds-stress distributions, $x/D = 75$. ○, $-\overline{uv}/U_m^2$; △, $-\overline{uw}/U_m^2$; □, wall shear stress measurements.

between intensities measured near each of the walls persists as a nearly constant displacement between the curves over a large part of the central flow.

Figure 12 shows streamwise intensities in the fully developed central flow. A similar, regular Reynolds number dependence is evident for the inner- and straight-wall flows, and may exist for the outer-wall flow if the discrepancies are due to the small errors in traverse positioning mentioned earlier.

Figure 13 gives a comparison of wall-region streamwise intensities. The similarity between profile shapes and their Reynolds number dependence is clear. Direct comparison of wall-region data for the three wall curvature cases at a single Reynolds number is given in figure 14. The displacement of the inner-wall data below, and the outer-wall data above, the straight-wall data is consistent with the earlier discussion of the turbulence energy equations. The results of Eskinazi & Yeh (1956) indicate a similar behaviour, with larger displacements compatible with their larger degree of curvature. The general level of their data is, however, much lower than that of the present results, which agree well with Comte-Bellot's data for straight duct flow when the same methods of shear velocity estimation are used.

The transverse turbulence intensities $\tilde{v}$ and $\tilde{w}$ in the central flow region are shown in figure 15. The data are similar for all three wall conditions, and both $\tilde{v}$ and $\tilde{w}$ exhibit

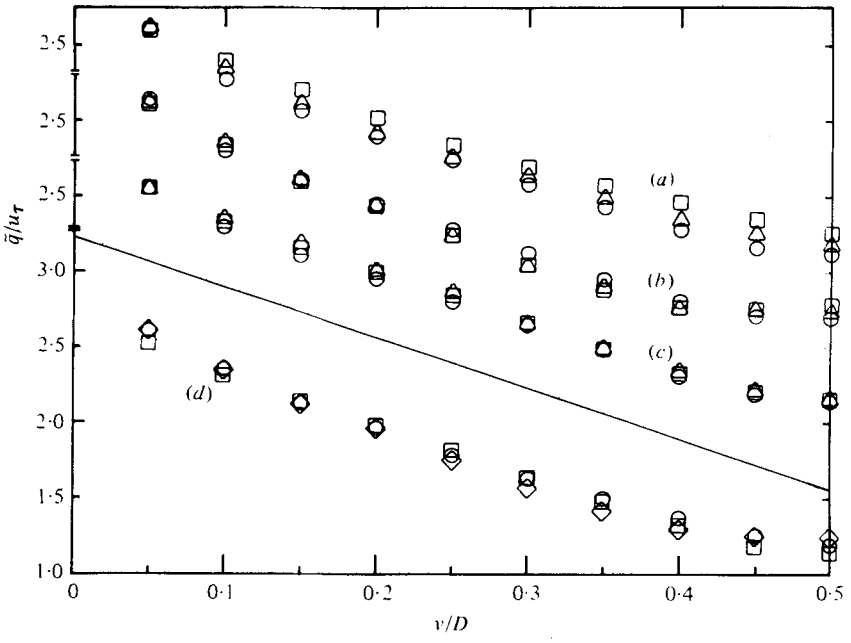

FIGURE 17. Total turbulence energy in the central region, $x/D = 75$. (*a*) Outer, (*b*) inner and (*c*) straight wall: ○, $R_N = 30000$; □, $R_N = 60000$; △, $R_N = 130000$. (*d*) Comparison of means: ○, outer wall; ◇, inner wall; □, straight wall.

a Reynolds number variation in the opposite sense to that found for the streamwise component $\tilde{u}$.

Figure 16 shows the measured distributions of Reynolds stresses $-\overline{uv}$ and $-\overline{uw}$, compared with the distributions expected from the wall shear measurements. The cross-wire technique is very sensitive to the existence of transverse mean velocities V and W, and cannot be corrected for these effects without a detailed knowledge of the yaw-angle distribution. The agreement within the inner flow region is therefore encouraging, and consistent with the conclusion of a very weak level of secondary flow, but the data for the outer region are probably better taken as confirmation of the existence of significant secondary flow levels, rather than as accurate measures of the shear-stress distributions.

One implication of the earlier discussion of the turbulence intensity equations is that complete similarity between the flows is obtained only in terms of the total turbulence energy $\frac{1}{2}\overline{q^2} = \frac{1}{2}(\overline{u^2}+\overline{v^2}+\overline{w^2})$, as it is only for this quantity, rather than the individual turbulence intensity components, that the equations are directly comparable. A similar proposition may be put for any one of the wall flow types for a range of Reynolds number variation: if a two-component turbulence model is considered, the scales determining the 'active' and 'inactive' components will have different levels of significance in determining each of the turbulence production, distribution and dissipation processes. For a range of low Reynolds numbers such as the present one, the ratios of active to inactive scales may vary significantly. It is then expected that the individual intensity components, which are all directly affected in complementary ways by the distributive processes, will exhibit much larger variation than the total turbulence energy, which encompasses the individual variations.

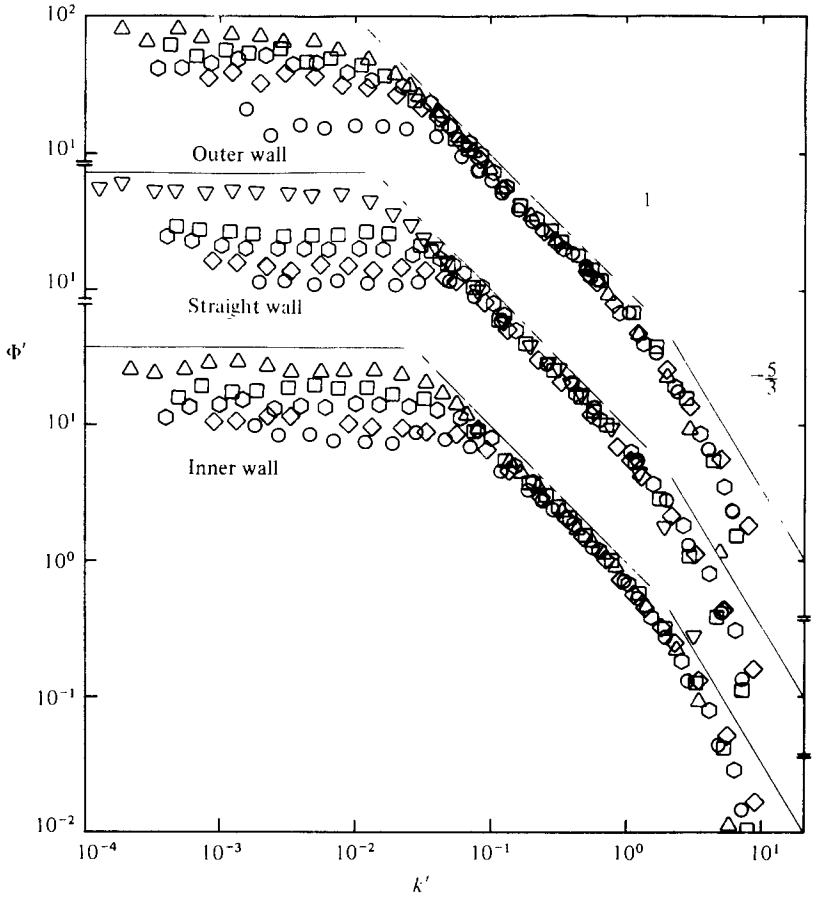

FIGURE 18. Logarithmic-region spectra.

	y^*	$R_N \times 10^{-3}$		y^*	$R_N \times 10^{-3}$
○	80	30	◇	160	60
□	80	60	△	160	130
▽	80	130	⬡	320	130

Tests of these propositions are shown in figure 17, where $\tilde{q} = (\overline{u^2} + \overline{v^2} + \overline{w^2})^{\frac{1}{2}}$. The straight-wall and inner-wall data (figure 17*b*, *c*) show comparatively little variation with Reynolds number. The wider scatter of the outer-wall data (figure 17*a*) essentially reflects the irregularities in the streamwise intensity component distributions (figure 12). The variation between data sets for the highest and lowest Reynolds numbers is small, and comparable to that for the other two wall conditions.

The means of the distributions for the three wall conditions are compared in figure 17(*d*). The duct width D was taken as a common length scale in view of the absence of any more justifiable scale for 'shear-dominated' flows. The agreement between the distributions is reasonably good for y/D less than approximately 0·3. The larger discrepancies evident for regions further from the wall may be attributed to the inadequacy of the common length scale, among other factors.

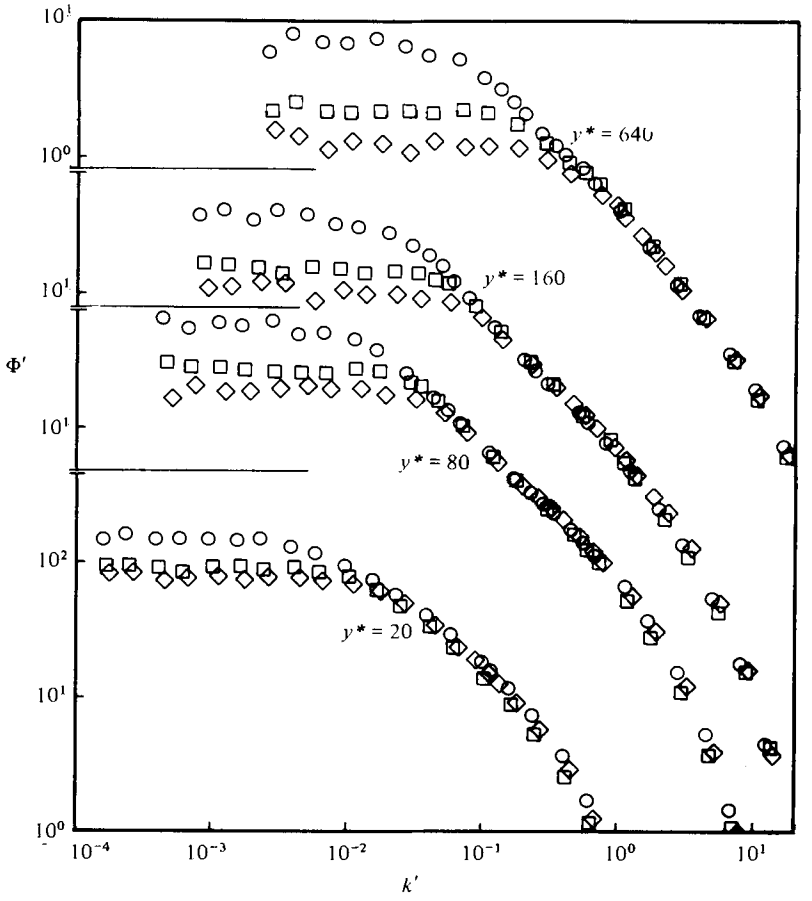

FIGURE 19. Comparison of spectra for inner-, outer- and straight-wall flows. $R_N = 60000$, y^* values as shown. ○, outer wall; ◇, inner wall; □, straight wall.

4.3. *Energy spectra*

To investigate further the viability of a two-component turbulence model for curved flows, spectra were measured for the streamwise intensity component $\overline{u^2}$ at a series of comparable positions and Reynolds numbers for which the mean flow and turbulence distributions were considered fully developed. The spectra are presented in the non-dimensional form Φ' *vs.* k', where

$$\int_0^\infty \Phi'[k', x_1, x_2, \ldots]dk' = \frac{\overline{u^2}}{u_\tau^2}[x_1, x_2 \ldots], \quad k' = ky.$$

Here Φ' is the non-dimensional intensity-normalized spectrum function, k' is the non-dimensional wavenumber and $x_1, x_2, \ldots$ are the further non-dimensional parameters required for description of the flow. The brackets denote a functional dependence. The streamwise, one-dimensional wavenumber $k = 2\pi f/U$, where f is frequency, by the usual Taylor-hypothesis definition.

The dimensionless wavenumber k' is that suggested by Townsend (1956) for correlation of spectra within the constant-stress layer. Perry & Abell (1975) confirmed that a near-invariant wavenumber range of the normalized spectrum occurred on this

basis for data taken in the logarithmic mean flow region of their pipe flow. The present data for the logarithmic mean flow region for each type of wall are shown in figure 18. In each case a clearly identifiable wavenumber range exists in which the spectrum function is of the form $\Phi' = Jk'^{-1}$, where the constant J is invariant with both position in the flow field and Reynolds number.

The range does not exist for data taken within the viscous region or within the central flow region (compare spectra for these regions given in figure 19). Kolmogorov-type inertial subranges, in which the spectrum function varies as $k^{-\frac{5}{3}}$, are not clearly definable for any of the spectra.

Figure 19 gives direct comparisons between spectra for the three different wall types, for a range of common dimensionless wall distances. The spectra demonstrate that the changes in streamwise turbulence intensity between the three flows are due to changes in intensity of the low wavenumber spectral components alone. The ratios (spectral intensity deviation/corresponding straight flow intensity) for low wavenumbers are larger for the outer-wall flow than for the inner wall flow, and increase as the central region is approached from each wall, in accordance with the earlier discussion. Instability in the spanwise position of the central flow structure could affect the low wavenumber ranges of the spectra. However, this would be expected to increase the measured low wavenumber levels of the inner- as well as the outer-region spectra, and the inner-region data do not support the possibility. The deviations are then taken to be due to changes in the turbulence processes as discussed earlier.

The data may be broadly described in terms of a two-component model such as that proposed by Townsend for the wall region. The universal, 'active' component determined by the turbulent shear stress may be considered to be responsible for the common, high wavenumber parts of the spectra. The spectra for $y^* = yu_\tau/\nu = 640$ correspond to $y/D = 0{\cdot}25$, and the active component is then seen to retain its significance in the central flow region.

Following Bradshaw's (1967) interpretation of the 'inactive' component as being determined by the large-scale turbulence in the central flow, the low wavenumber differences between the spectra may be attributed to differences between the central-region flows, the most obvious of which in the present case is the existence of the Taylor–Goertler vortex array in the curved flow. A further implication then is that the effect of streamline curvature in all flow regions is controlled by changes in the central flow structure, rather than by changes in local stability or mixing-length parameters.

5. Conclusions

The data obtained here for a duct flow with very small curvature exhibit significant differences from those for straight duct flow. A further distinction seems necessary between the present 'shear-dominated' type of flow and the more highly curved, 'inertia-dominated' flows investigated in the past. Mean flow behaviour in the present case cannot be described by the central-flow similarity laws which have had some success for highly curved flows, while the conventional straight-wall form of the law of the wall gives good correlation of the present wall-region data. A structure interpreted as a Taylor–Goertler vortex array was detected in the central region of the duct, and was similar to structures found in recent investigations of curved boundary layers.

An investigation of the momentum, energy and Reynolds-stress equations suggests that a significant mechanism by which the effects of streamline curvature are manifested is one of conservative reorientation of turbulent energy components, leading to changes in shear stress and a further 'feedback' effect through intensity changes. There is then no need to propose additional, particularly 'negative', turbulence energy production mechanisms, and a consistent interpretation of the equations for straight, curved and rotating flows is obtained. The interpretation also allows an estimate of the constant in Bradshaw's curvature model to be developed from straight flow data, and the estimate is close to the value he recommends.

The measured turbulence intensities follow a pattern generally consistent with the interpretation. In particular, the distribution of total turbulence energy in the central region exhibits comparatively little variation with either changes in Reynolds number or changes in wall curvature, even though the data for the separate intensity components show significant variations.

Energy spectra for the streamwise component are readily interpreted on the basis of a two-component turbulence model similar to that proposed by Townsend. A common, high wavenumber spectral range occurs for the corresponding spectra for inner, outer and straight wall flows, and is attributed to the 'active' component of the model, which then retains its significance in all flow regions. Differences between corresponding spectra are confined to the low wavenumber ends of the spectra, and are attributed to changes in the central-region large-scale turbulence structure, by comparison with Bradshaw's interpretation of the 'inactive' component. This implies that the effects of streamline curvature throughout the flow are determined by the central region structure alone.

REFERENCES

Batchelor, G. K. 1967 *An Introduction to Fluid Dynamics*. Cambridge University Press.

Bradshaw, P. 1967 *J. Fluid Mech.* **30**, 241.

Bradshaw, P. 1969 *J. Fluid Mech.* **36**, 177.

Bradshaw, P. 1972 *AGARD Conf. Proc.* no. CP-93, p. C-1.

Bradshaw, P. 1973 *AGARDograph* no. 169.

Bradshaw, P., Ferriss, D. H. & Atwell, N. P. 1967 *J. Fluid Mech.* **28**, 593.

Clauser, F. H. 1954 *J. Aero. Sci.* **21**, 91.

Coles, D. E. 1968 *Proc. AFOSR–IFP–Stanford Conf. Comp. Turbulent Boundary Layers*, vol. 2.

Comte-Bellot, G. 1963 Thesis, University of Grenoble. (Translated by P. Bradshaw as *ARC Rep.* no. 31 609, 1969.)

Ellis, L. B. & Joubert, P. N. 1974 *J. Fluid Mech.* **62**, 65.

Eskinazi, S. & Erian, F. F. 1969 *Phys. Fluids* **12**, 1988.

Eskinazi, S. & Yeh, H. 1956 *J. Aero. Sci.* **23**, 23.

Halleen, R. M. & Johnston, J. P. 1967 *Stanford University Dept. Mech. Eng. Thermosci. Div. Rep.* MD-18.

Hinze, J. O. 1959 *Turbulence. An Introduction to its Mechanism and Theory*. McGraw-Hill.

Hunt, I. A. & Joubert, P. N. 1977 Turbulent flow in a rectangular duct. *6th Austral. Hydraul. Fluid Mech. Conf., IEAust, Adelaide*, pp. 403–406.

Hunt, I. A. & Joubert, P. N. 1978 *Univ. of Melbourne, Mech. Engng Dept. Rep.* FM-8.

Irwin, H. P. A. H. & Smith, P. A. 1975 *Phys. Fluids* **18**, 624.

Johnston, J. P., Halleen, R. M. & Lezius, D. K. 1972 *J. Fluid Mech.* **56**, 533.

Kármán, T. von 1951 *Collected Works*, vol. 4, p. 452. Butterworths.

KIM, H. T., KLINE, S. J. & REYNOLDS, W. C. 1971 *J. Fluid Mech.* **50**, 133.

KINNEY, R. B. 1967 *Trans. A.S.M.E.* E **34**, 437.

KLINE, S. J., REYNOLDS, W. C., SCHRAUB, F. A. & RUNSTADLER, P. W. 1967 *J. Fluid Mech.* **30**, 741.

LAUFER, J. 1950 *N.A.C.A. Tech. Note* no. 2123.

LEZIUS, D. K. & JOHNSTON, J. P. 1971 *Stanford Univ. Dept. Mech. Engng Thermosci. Div. Rep.* MD-29.

MARRIS, A. W. 1956 *Can. J. Phys.* **34**, 1134.

MARRIS, A. W. 1960 *Trans. A.S.M.E.* D **82**, 528.

MERONEY, R. N. & BRADSHAW, P. 1975 *A.I.A.A. J.* **13**, 1448.

MOON, I. M. 1964 *Gas Turbine Lab. MIT, Rep.* no. 74.

MORRISON, G. L., PERRY, A. E. & SAMUEL, A. E. 1972 *J. Fluid Mech.* **52**, 465.

PATEL, V. C. 1965 *J. Fluid Mech.* **23**, 185.

PATEL, V. C. 1968 *Aero. Res. Counc. Current Paper* no. 1043.

PATEL, V. C. & HEAD, M. R. 1969 *J. Fluid Mech.* **38**, 181.

PERRY, A. E. & ABELL, C. J. 1975 *J. Fluid Mech.* **67**, 257.

PERRY, A. E. & MORRISON, G. L. 1971*a* *J. Fluid Mech.* **47**, 577.

PERRY, A. E. & MORRISON, G. L. 1971*b* *J. Fluid Mech.* **47**, 765.

PRANDTL, L. 1931 *N.A.C.A. Tech. Mem.* no. 625.

ROTTA, J. C. 1967 *Phys. Fluids Suppl.* **9**, S174.

SMITH, A. M. O. 1955 *Quart. Appl. Math.* **13**, 233.

SO, R. M. C. & MELLOR, G. L. 1975 *Aero. Quart.* **26**, 25.

TANI, I. 1962 *J. Geophys. Res.* **67**, 3075.

TAYLOR, G. I. 1923 *Phil. Trans.* A **223**, 289.

TOWNSEND, A. A. 1956 *The Structure of Turbulent Shear Flow*. Cambridge University Press.

TOWNSEND, A. A. 1961 *J. Fluid Mech.* **11**, 97.

TRAUGOTT, S. C. 1958 *N.A.C.A. Tech. Note* no. 4135.

WATTENDORF, F. L. 1935 *Proc. Roy. Soc.* A **148**, 565.

WYNGAARD, J. C. 1968 *J. Phys.* E **1**, 1105.

YEH, H., ROSE, W. G. & LIEN, H. 1956 *Final Rep. to ONR Contract* NONR-248(33). Johns Hopkins Univ.